Self-Assembling Amphiphilic Peptides Target the VDAC1-Hexokinase-II Complex to Induce Apoptosis in Cervical Carcinoma Cells

Wanfeng Sun, Angelina Angelova, Xintong Han, Xibai Wang, Borislav Angelov, Qibin Chen, Na Li, Aihua Zou

Self-Assembling Amphiphilic Peptides Target the VDAC1-Hexokinase-II Complex to Induce Apoptosis in Cervical Carcinoma Cells

Wanfeng Sun[a], Angelina Angelova[b], Xintong Han[c], Xibai Wang[c], Borislav Angelov[d], Qibin Chen[a], Na Li[e*], Aihua Zou[c,a*]

[a]School of Chemistry and Molecular Engineering, East China University of Science and Technology, Shanghai 200237, China

[b]Université Paris-Saclay, CNRS, Institut Galien Paris-Saclay, F-91400 Orsay, France

[c]College of Chemistry and Materials Science, Shanghai Normal University, 100 Guilin RD, Shanghai 200234, China

[d]Extreme Light Infrastructure ERIC, Department of Structural Dynamics, CZ-25241 Dolni Brezany, Czech Republic

[e]National Facility for Protein Science in Shanghai Zhangjiang Laboratory, Shanghai Advanced Research Institute, CAS, Shanghai 20124, China

KEYWORDS: VDAC1-derived peptides, Cell-penetrating peptides (CPP), Self-assembly, Mitochondria-mediated apoptosis, Cervical carcinoma

ABSTRACT

VDAC1, an outer mitochondrial membrane protein overexpressed in cancers, regulates apoptosis by interacting with anti-apoptotic proteins and releasing apoptotic factors. We investigate novel multi-block cationic peptide amphiphiles targeting the VDAC1-Hexokinase-II complex in the mitochondria of cervical carcinoma cells. Amphiphilic peptide variants were designed by modifying the C-terminal of VDAC1 fragment LP1 with a cationic hydrophilic segment and the N-terminal with a hydrophobic domain, enabling self-assembly into nanofiber-like structures at elevated concentrations. In HeLa cells, these peptides triggered mitochondrial-mediated apoptosis through a decrease of mitochondrial membrane potential, cytochrome C release, and caspase activation, suggesting disrupted VDAC1-HK-II interaction. The mitochondria-targeting peptides showed notable selective cytotoxicity to cancer cells with minimal effects on normal 3T3 cells. Our findings demonstrate that amphiphilic peptides for VDAC1-HK-II-targeting represent a promising mitochondria-focused therapeutic strategy for cervical cancer inhibition, combining structural self-assembly properties with enhanced apoptotic efficacy in malignant cells.

INTRODUCTION

Chemotherapy is one of the primary methods employed in cancer treatment. However, conventional chemotherapeutic agents exhibit numerous limitations, including poor solubility, low bioavailability, rapid blood clearance, susceptibility to drug resistance, inadequate cellular absorption, and significant side effects on healthy subjects, *etc*[1]. To address these challenges, several targeted drugs and drug delivery systems have been developed to enhance drug accumulation at tumor cells while minimizing adverse effects on healthy tissues[2,3]. Among these innovations, peptide-based drugs have emerged as bio-nanomaterials characterized by good biocompatibility, tailorable molecular design, and specific biorecognition ability of target molecules[4]. Notably, non-covalent interactions such as hydrogen bonding, hydrophobic interactions, and π-π stacking[5,6] facilitate the self-assembly of amphiphilic peptides into nanostructures, including nanoparticles[7], nanofibers[8,9], and nano-gels[10]. The self-assembly of peptides into nanostructures can significantly enhance their stability and targeting capabilities[11]. The primary target sites for these nanostructures include the vasculature, cellular microenvironment, cell membrane, cytoplasm and organelles[12]. These advantageous properties

have attracted significant attention and are being explored to develop novel functional bio-nanomaterials for cancer therapy. [13,14].

Mitochondria are essential organelles that play a crucial role in a variety of biological processes[15,16], including the regulation of cell survival and apoptosis[17,18]. Mitochondrial-mediated apoptosis typically occurs due to mitochondrial damage, which results in alterations in membrane permeability and the release of cytochrome C into the cytoplasm. This release activates caspases and other apoptotic signals[19–21]. In this regard, specific targeting of the mitochondria of cancer cells to activate mitochondria-mediated apoptosis presents a promising strategy for cancer treatment.

The interactions between anti-apoptotic proteins and the release of apoptotic proteins render VDAC1 a crucial component in mitochondria-mediated apoptosis. Located at the outer mitochondrial membrane (OMM), VDAC1 is overexpressed in various cancer cell types. Accumulating evidence indicates that it is a significant target for mitochondria-targeted anticancer strategies. VDAC1, as a class of pore proteins in the OMM, serves as a crucial regulator of mitochondrial function. Additionally, it modulates metabolism and energy transfer between mitochondria and other cellular components. VDAC1 plays diverse roles in the apoptosis process by interacting with various proteins. For instance, VDAC1 interacts with anti-apoptotic proteins such as Hexokinase-II (HK-II) and Bcl-2, which protect cells from apoptosis.

Studies have demonstrated that the expression of HK-II in cancer cells is significantly elevated compared to normal cells[22,23]. The overexpressed HK-II interacts with VDAC1 on the mitochondrial outer membrane, promoting cancer cell proliferation and inhibiting the apoptosis. Consequently, targeting mitochondria to facilitate the separation of HK-II from VDAC1 to induce apoptosis represents a promising cancer treatment strategy[24]. Traditional small-molecule drugs face challenges in disrupting protein-protein interactions due to the extensive interfaces and narrow grooves involved[25]. In contrast, peptides offer advantages such as high selectivity, efficiency, and relative safety[26]. Current research is rapidly advancing in the development of protein mimetic peptide amphiphiles and therapeutic peptides for hampering the VDAC1-Hexokinase-II protein complex[27,28,29]. The purpose is to propose anticancer agents with favorable bioavailability and biodegradability.

Recently, an amphiphilic self-assembling peptide based on HK-II, Pal-pHK-pKV, has demonstrated significant potential in promoting the separation of VDAC1 and HK-II, thereby inducing apoptosis[27,28]. Shoshan Barmatz and co-workers have identified a series of VDAC1-based peptides[29], and investigated the antitumor properties of LP4-series peptides (KKLETAVNLAWTAGNSN) and N-terminal series variants (RDVFTKGYGFGL)[30–32]. Zhang *et al*.[33] have utilized the N-terminal peptide as the template, and modified the cationic and hydrophobic blocks to create three amphiphilic self-assembled cationic peptides (pFL-N-Ter-TAT, Pal-N-Ter-TAT and Pal-pFL-N-Ter-TAT). The performed studies have indicated that this series of peptides can effectively target mitochondria and induce the separation of HK-II and VDAC1, thereby facilitating apoptosis.

We designed specific alterations to the VDAC1 protein fragment LP1 by anchoring a hydrophilic cationic fragment (TAT or RVR) to the C-terminus and a hydrophobic fragment (palmitic acid or pFL) to the N-terminus (see Table 1 below). We hypothesized that these multi-block peptides could effectively target the HK-II-VDAC1 complex on mitochondria, thereby promoting the dissociation of HK-II and facilitating mitochondria-mediated apoptosis. The self-assembled morphology and secondary structure of the peptides were characterized using Transmission Electron Microscopy (TEM) and circular dichroism (CD) spectroscopy. Consequently, we conducted several biological experiments to demonstrate that the VDAC1-based amphiphilic peptides can effectively target the VDAC1-HK-II complex on the mitochondria of HeLa cells, inducing the dissociation of HK-II from the mitochondria and subsequently triggering mitochondria-mediated apoptosis. Our purpose is to develop amphiphilic peptides that target the VDAC1-HK-II complex in cervical cancer cells, disrupting these protein interactions to induce mitochondria-mediated apoptosis, and enhance therapeutic efficacy.

RESULTS AND DISCUSSION

Peptide design rationale

We targeted the VDAC1-Hexokinase-II complex at the outer mitochondrial membrane of cervical carcinoma cells using newly designed cationic peptides aiming at inhibiting cancer cell

proliferation. To obtain amphiphilic peptide derivatives of self-assembly propensity, we modified the C-terminal of the VDAC1 protein fragment LP1 (WTEYGLTFTEKWNTDN) by anchoring a hydrophilic cationic fragment and the N-terminal with a hydrophobic fragment. Hydrophobic palmitic acid (Pal) or a hydrophobic peptide sequence pFL were anchored at the N-terminus of LP1 to enhance the peptide's amphiphilicity. To enhance cellular uptake, we incorporated the cell-penetrating peptides (CPPs) TAT (GRKKRRQRRRPQ) and RVR (RRRRNRTRRNRRRVR) at the C-terminus of the LP1-derived sequences. These cationic CPPs are known to facilitate the internalization of peptides into cells, a crucial prerequisite for reaching the intracellular target, the mitochondria. The hydrophilic cationic fragments TAT and RVR were conjugated to the C-terminus of LP1, which increased the cationic charge of the designed peptide and favored the interaction with the negatively charged lipid membranes.

Our investigation explores multiple peptide variants (pFL-LP1-TAT, Pal-LP1-TAT, and Pal-LP1-RVR) presented in Table 1, highlighting the diverse potential avenues for cervical cancer treatment.

Table 1. Conceived sequences of amphiphilic mitochondrial VDAC1-based peptides comprised by two or three building blocks.

Peptide	Sequence	MW	Charge at pH7
LP1	WTEYGLTFTEKWNTDN	2004	-2
LP1-TAT	WTEYGLTFTEKWNTDNGRKKRRQRRRPQ	3607	+6
pFL-LP1-TAT	FPWWWPFLWTEYGLTFTEKWNTDNGRKKRRQRRRPQ	4766	+6
Pal-LP1-TAT	Pal-WTEYGLTFTEKWNTDNGRKKRRQRRRPQ	3845	+6
Pal-LP1-RVR	Pal-WTEYGLTFTEKWNTDNRRRRNRTRRNRRRVR	4389	+9

Whereas the VDAC1-based peptide LP1 has a negative net charge (-2), the modified peptides LP1-TAT, pFL-LP1-TAT, Pal-LP1-TAT, and Pal-LP1-RVR involved cationic cell-penetrating aminoacid sequences (TAT or RVR), which imparted a positive net charge to the conjugates (Table 1). We hypothesized that the novel positively charged amphiphilic peptides can self-assemble,

above critical concentration, into nanostructures driven by hydrophobic interactions, hydrogen bonding, electrostatic, and van der Waals forces (Scheme 1).

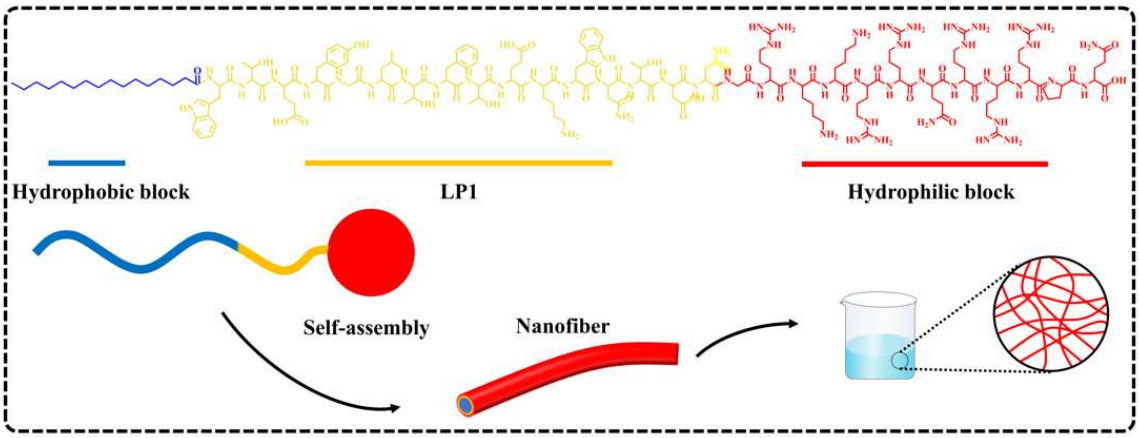

Scheme 1. Chemical structure of the designed modified LP1 peptide, derived from VDAC1, and self-assembly of the multi-block amphiphilic peptide to form nanofibers. In this design, a hydrophobic palmitic acid (Pal) tail (or a hydrophobic peptide sequence (pFL)) is conjugated at the N-terminus of LP1. Hydrophilic cationic fragments (TAT or RVR) are incorporated into the C-terminus of the LP1 peptide to impart amphiphilicity and cell-penetrating properties.

Determination of critical micelle concentration (CMC)

The critical micelle concentration (CMC) was determined using a pyrene fluorescent probe, based on the curve of the fluorescent intensity ratio (I_1/I_3) *versus* concentration. The results are presented in Figure S1. The CMC values for the peptides pFL-LP1-TAT, Pal-LP1-TAT, and Pal-LP1-RVR were estimated to be 91.2, 81.2, and 56.3 μM, respectively.

Nanoassembly formation

The self-assembly behavior of the multi-block amphiphilic peptides (Table 1) was investigated in an aqueous medium. The peptides LP1 and LP1-TAT were highly soluble and did not exhibit self-assembly behavior due to the lack of amphiphilic properties. The absence of hydrophobic moieties and segments is expected to affect their interaction with the cellular membranes[34].Our *in vitro* biological assays were conducted at concentrations below the CMC to

specifically investigate the activity of the monomeric peptide, which we hypothesize is the primary bioactive species responsible for cellular uptake and target engagement.

The nanoassembly morphology was examined using TEM at a concentration of 500 μM (Figure 1). The concentration of 500 μM is well above the determined CMC values. This higher concentration was used to ensure clear visualization of the self-assembled nanostructures. While the CMC represents the concentration at which self-assembly begins, it does not preclude the presence of assembled structures at higher concentrations. Above the CMC, the equilibrium shifts towards the assembled state, and different morphologies can be observed depending on the peptide concentration.

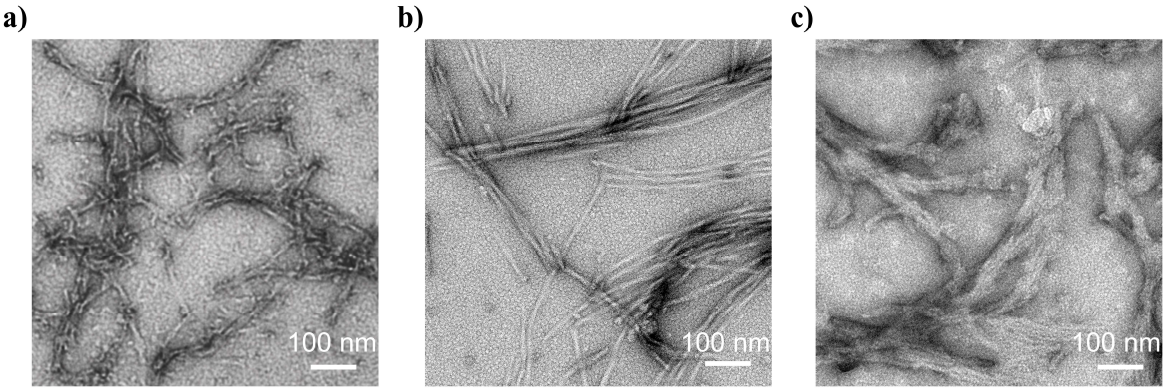

Figure 1. TEM images of the designed mitochondrial VDAC1-based amphiphilic peptides: a) pFL-LP1-TAT (500 μM), b) Pal-LP1-TAT (500 μM), and c) Pal-LP1-RVR (500 μM).

The TEM images in Figure 1 show that the peptides pFL-LP1-TAT and Pal-LP1-TAT self-assemble to form nanofibers with average widths of 8 nm and 11 nm, respectively (Figures 1a and 1b). In contrast, the peptide Pal-LP1-RVR formed nanofiber assemblies with an average width of approximately 40 nm (Figure 1c). The significant difference in the nanofibers' width between Pal-LP1-RVR and the other two peptides may be due to the different charge properties (Table 1). Increased cationic character may lead to stronger repulsion between molecules, resulting in a larger fiber diameter. Therefore, the observed differences in the fiber diameters may be attributed to variations in charge repulsion, packing within the fibers, and the potential formation of higher-order aggregates. The factors governing fiber sizes would require separate studies. It would be of interest to investigate whether the self-assembled nanofibers may enhance the therapeutic effect at

elevated peptide concentrations through more effective displacement of HK-II from VDAC1. In fact, the self-assembled nanofibers may provide a protective environment for the peptides, safeguarding them against enzymatic degradation and prolonging their bioactivity at biological barriers, acting as a reservoir for the sustained release of active monomers.

Our hypothesis in this study is as follows: The monomeric peptide is the primary bioactive species that penetrates the cell membrane and disrupts the VDAC1-HK-II complex. The ability to self-assemble into nanofibers at higher concentrations (above the CMC) is a crucial formulation feature that provides a "depot" or "reservoir" effect. This reservoir can protect the peptides from enzymatic degradation in a complex biological environment and ensure a sustained release of active monomers, which is particularly relevant for *in vivo* applications.

Peptide conformation

The secondary structures of the VDAC1-based amphiphilic peptides at varying concentrations were investigated using CD spectroscopy (Figure 2 and Fig S4). The CD spectra of the peptides in Figures 2b and 2c displayed double negative peaks at wavelengths near 208 nm and 222 nm, which are characteristic of α-helical structures. As expected, the CD spectra were concentration dependent. Considering that the CMC values for the peptides pFL-LP1-TAT, Pal-LP1-TAT, and Pal-LP1-RVR are 91.2, 81.2, and 56.3 μM, respectively, the formation of self-assembled peptide aggregates (nanofibers) at concentrations above the CMC, may reduce the CD signal and hamper the quantitative analysis of secondary structure content. For the studied concentration range, the data in Figure 2 did not show molar ellipticity decrease with increasing peptide concentration.

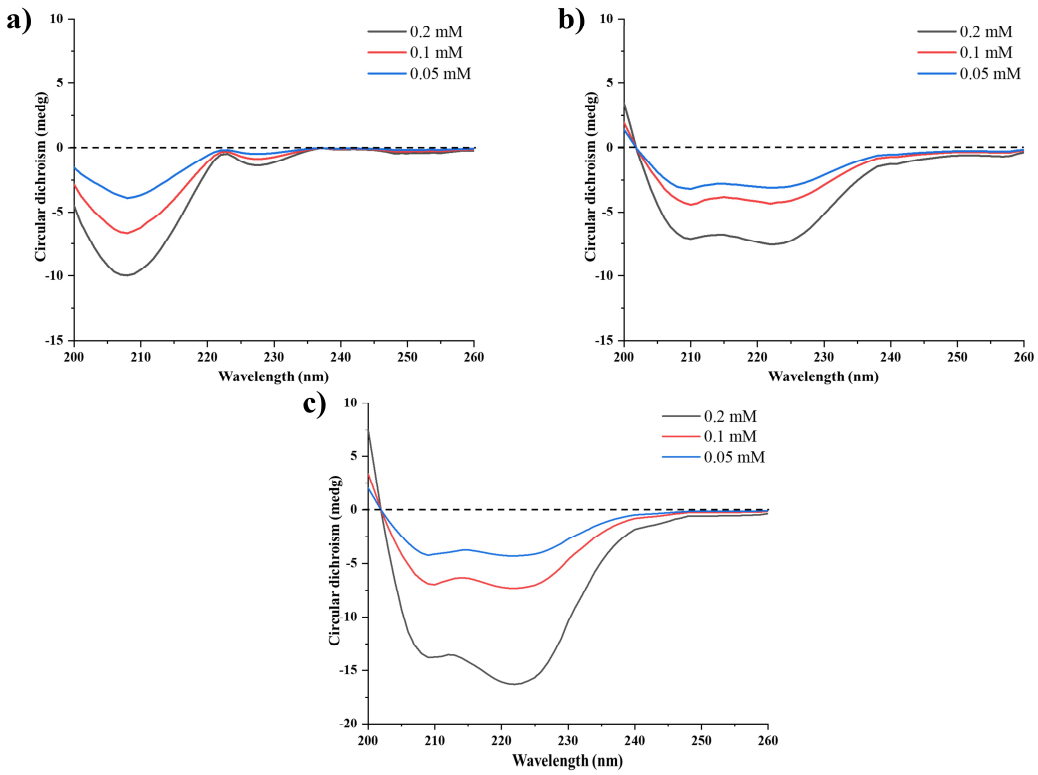

Figure 2. CD spectra of multi-block peptides at concentrations 50, 100, and 200 μM in the aqueous phase: a) pFL-LP1-TAT, b) Pal-LP1-TAT and c) Pal-LP1-RVR.

The quantitative percentages of the present peptide conformations were assessed using two different algorithms (Tables S1 and S2). The results revealed that the helicity of pFL-LP1-TAT was lower than that of Pal-LP1-TAT, and the helicity of Pal-LP1-TAT was also lower than that of Pal-LP1-RVR. Furthermore, we calculated the ratio of the molar ellipticity $\theta_{222}/\theta_{208}$, which serves as an additional measure of the α-helical content of the peptides. A ratio of $\theta_{222}/\theta_{208} \geq 1$ characterizes coil-coil organization in solution, whereas $\theta_{222}/\theta_{208} \leq 0.86$ is expected for isolated helices[35]. The ratio of $\theta_{222}/\theta_{208}$ for pFL-LP1-TAT was found to be lower than 0.86, while those for Pal-LP1-TAT and Pal-LP1-RVR exceeded 1. These results suggest that pFL-LP1-TAT exists as isolated helices, whereas Pal-LP1-TAT and Pal-LP1-RVR adopt coiled coil conformations (Table S3). The observed differences imply that the incorporation of a fatty acid tail into the peptide may enhance the stability of the α-helical conformation[36]. Additionally, it is known that the α-helical conformation facilitates the peptide insertion into lipid membranes, thereby aiding in the traversal of biological membrane barriers[27,33,37].

Cytotoxicity to cancer (HeLa) and normal (3T3) cells

Cellular viability experiments were performed at peptide concentrations of up 50 μM, *i.e.,* in a non-aggregated molecular state. The CMC values for the peptides pFL-LP1-TAT, Pal-LP1-TAT, and Pal-LP1-RVR were 91.2, 81.2, and 56.3 μM, respectively (Fig. S1). It is important to note that these concentrations are below the measured CMC values in PBS, indicating that the peptides were primarily in their monomeric form during these experiments, allowing for the assessment of the intrinsic activity of the peptide molecules. However, the apparent CMC could be lower in the complex environment of the cell culture medium.

This study was performed under the assumption that the peptides were primarily in monomeric forms during the cytotoxicity experiments. Three types of cancer cells of HeLa, A375. and A549 were treated with the amphiphilic peptides pFL-LP1-TAT, Pal-LP1-TAT, and Pal-LP1-RVR at various concentrations for 24 h. The cell viability of HeLa cells was assessed using MTT assays (Figure 3). At the highest concentration (50 μM), over 90% of the HeLa cells exhibited considerable viability after 24 h of incubation with the peptides LP1 and LP1-TAT, indicating low toxicity for these peptides. This suggested that the limited amphiphilicity of LP1 and LP1-TAT hinders their ability to penetrate the cancer cell barriers and reach subcellular sites of action on the OMM[34].

In contrast, HeLa cells treated with amphiphilic cationic peptides displayed a dose-dependent decrease in cellular viability (Figure 3a). Particularly, only 3.97%, 3.65%, and 3.17% of HeLa cells remained viable after 24 h of incubation with peptides pFL-LP1-TAT, Pal-LP1-TAT, and Pal-LP1-RVR at a concentration of 50 μM, respectively.

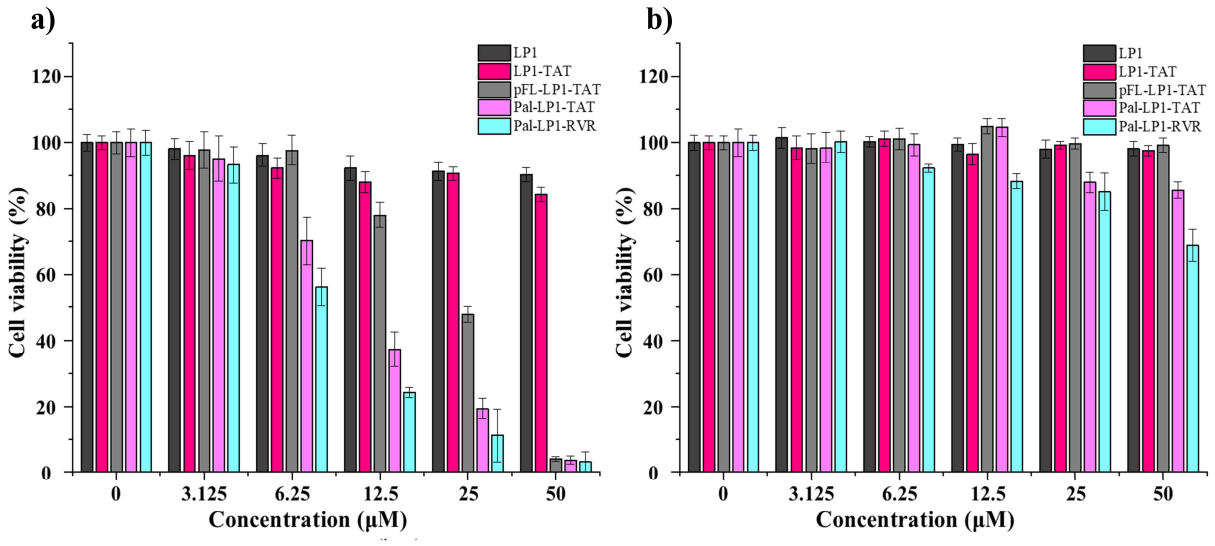

Figure 3. Determination of cellular viability with MTT assays. a) HeLa cells, and b) 3T3 cells were treated with different concentrations of peptides LP, LP1-TAT, pFL-LP1-TAT, Pal-LP1-TAT and Pal-LP1-RVR for 24 h. Untreated cells were measured as a control. The designed peptides exhibited minimal toxicity to normal 3T3 cells. The data were presented as mean ± SD (n= 3).

The half maximal inhibitory concentration (IC_{50}) values for pFL-LP1-TAT, Pal-LP1-TAT, and Pal-LP1-RVR in HeLa cells after 24 h of treatment were determined to be 24.8 ± 0.4 μM, 6.8 ± 0.7 μM, and 4.9 ± 0.5 μM, respectively (Table 2). These results suggested that the amphiphilic peptides, involving both hydrophobic and hydrophilic building blocks, interact more strongly with biological membrane barriers[27,28,33,34]. Subsequently, A375 and A549 cells were treated with amphiphilic peptides at various concentrations for 24 hours, and the IC_{50} values were calculated, as shown in Table 2. The results indicated that all amphiphilic peptide variants exhibit significant anticancer activity across the three cancer cell lines, with the highest toxicity observed in HeLa cells. Consequently, HeLa cells were selected as the focus of further research.

Table 2. Half maximal inhibitory concentration (IC_{50}) values, determined from 24h-cytotoxicity against HeLa cells, and correlating with the molecular structures of the designed peptides.

Peptide	IC_{50} (μM)

pFL-LP1-TAT	24.8±0.4
Pal-LP1-TAT	6.8±0.7
Pal-LP1-RVR	4.9±0.5

Importantly, the peptide Pal-LP1-RVR exhibited a minimal effect on the viability of normal 3T3 mouse fibroblast cells even at the highest investigated concentration of 50 μM (Figure 3b). The other mitochondrial VDAC1-based peptides demonstrated low cytotoxicity to normal 3T3 cells. The data in Figures 3a and 3b illustrated that the designed mitochondrial VDAC1-derived peptides significantly inhibit the proliferative activity of HeLa cells, with a markedly stronger effect as compared to their influence on normal 3T3 cells. These findings suggest that mitochondrial VDAC1-based peptides can effectively target the overexpressed proteins located at the OMM of cancer cells. Furthermore, it can be inferred that these peptides hold considerable potential for safe cervical cancer inhibition.

Mitochondria-mediated apoptosis

We further investigated whether the amino acid modifications introduced in the newly designed peptides enhance their ability to target the VDAC1-Hexokinase-II complex on the outer mitochondrial membrane. To assess whether this targeting mechanism induces mitochondria-mediated apoptosis in the examined cancer cells, we conducted an Annexin V-FITC/PI apoptosis assay. For *in vitro* studies, peptide concentrations of 12.5 μM were used. This concentration is below the CMC of the peptides, suggesting that they interact in a monomeric state. The Annexin V-FITC/PI apoptosis detection kits was employed to investigate the apoptotic effects of amphiphilic self-assembled peptides pFL-LP1-TAT, Pal-LP1-TAT, and Pal-LP1-RVR on HeLa cells, utilizing flow cytometry (Figure 4). HeLa cells were treated with 12.5 μM of each peptide for 4 hours. The 4-hour time point was chosen to capture early apoptotic events, such as changes in mitochondrial membrane potential and cytochrome C release.

The results indicated that the total apoptosis rate for cells incubated with pFL-LP1-TAT was 20.6%, while the apoptosis rates for cells treated with Pal-LP1-TAT and Pal-LP1-RVR were 77.0% and 82.6%, respectively. These findings suggest that the designed amphiphilic peptides induce cell death in HeLa cells through the apoptotic pathway.

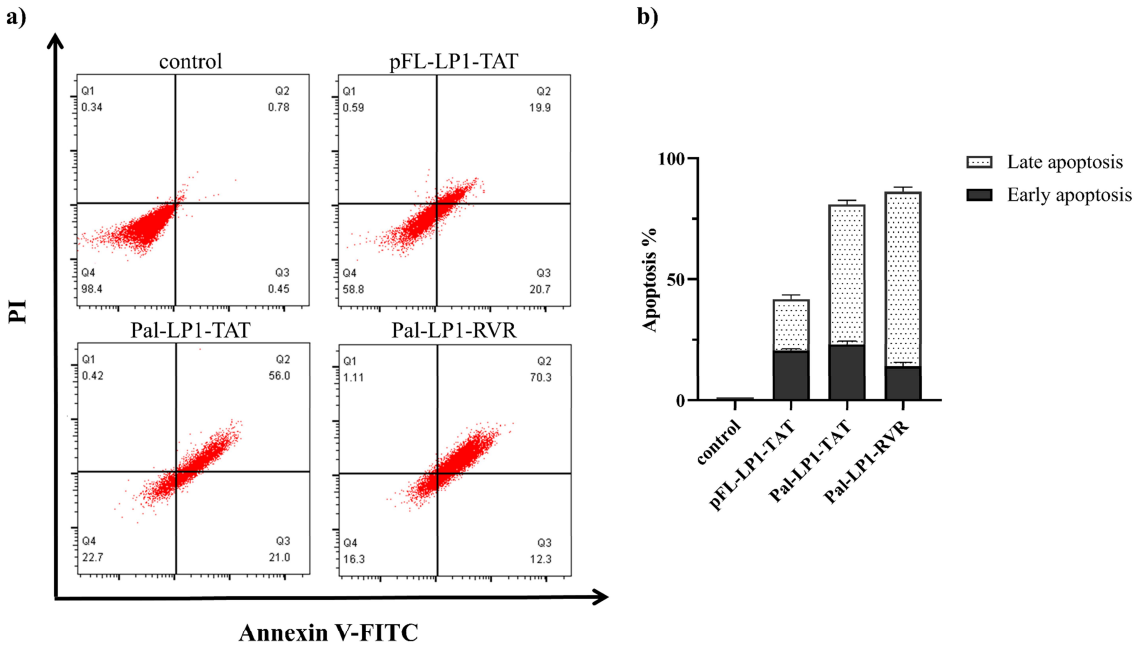

Figure 4. a) Cell apoptosis analysis after Annexin V-FITC/PI staining by flow cytometry. b) A summary of the incidence of early apoptosis, late apoptosis, and total apoptosis in HeLa cells. Data was presented as mean ± SD (n = 3).

The amphiphilic cationic peptides Pal-LP1-TAT and Pal-LP1-RVR, which possess a higher positive charge and helicity, demonstrated an enhanced capacity to trigger apoptosis in HeLa cells by targeting mitochondria and inducing the dissociation of HK-II from VDAC1 on the OMM. This process initiates mitochondria-mediated apoptosis, thereby presenting new opportunities for the development of mitochondria-targeting amphiphilic peptides in anticancer strategies.

Intracellular localization and mechanism of action

The intracellular localization of novel amphiphilic cationic peptides upon uptake by HeLa cells was investigated using confocal fluorescence microscopy. The designed peptides were labeled with FITC, which emits a green fluorescence signal when excited by a laser (Figure 5a). HeLa cells were exposed to 12.5 μM of the peptides pFL-LP1-TAT, Pal-LP1-TAT, and Pal-LP1-RVR for 4 hours. The green fluorescence signal in HeLa cells treated with pFL-LP1-TAT was significantly weaker as compared to those treated with Pal-LP1-TAT and Pal-LP1-RVR,

indicating insufficient uptake of pFL-LP1-TAT. Conversely, a strong green fluorescence signal was observed in HeLa cells incubated with Pal-LP1-TAT and Pal-LP1-RVR, suggesting a considerable increase in the cellular uptake of these amphiphilic cationic peptides. The varying intensities of the green fluorescence signals in cancer cells incubated with these VDAC1-based peptides were correlated with the amphiphilic structure of the peptides, which aligns with the results of cell apoptosis assays. Figure 5a illustrates the distribution of red fluorescence from the mitochondria-targeting dye in treated HeLa cells, alongside the green fluorescence of the FITC-labelled amphiphilic cationic peptides pFL-LP1-TAT, Pal-LP1-TAT, and Pal-LP1-RVR that were internalized by the cells. The presence of yellow fluorescence in the images indicates the colocalization of the internalized peptides (green) with the mitochondria (red) of the treated HeLa cells (merged images). The confocal microscopy images obtained demonstrate that the designed VDAC1-based amphiphilic cationic peptides induce apoptosis in HeLa cells by targeting their mitochondria. The primary localization effect arises from the LP1 sequence itself, which is derived from VDAC1. Our confocal microscopy results confirmed this localization through evidencing colocalization of the fluorescently labeled peptides with the mitochondrial markers.

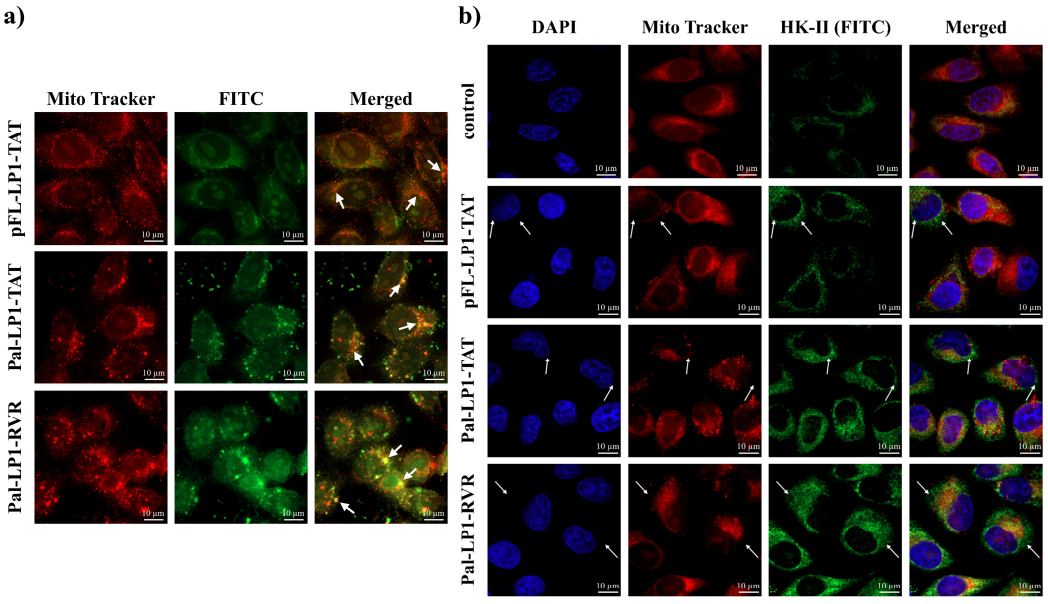

Figure 5. a) Confocal microscopy images of intracellular localization of the designed peptides. The green fluorescence is due to the uptake of the FITC-labeled peptides, which concentrate inside the cells. The red fluorescence is associated with the mitochondrial staining. The arrows indicate the colocalization on the merged images. b) Confocal microscopy images of the detachment of mitochondria-bound HK-II. The blue fluorescence is associated with the dye location in the nucleus. The green fluorescence indicates the HK-II distribution by immunostaining. The red

fluorescence shows the location of the mitochondria. The arrows indicate the detachment of HK-II from the mitochondria.

To further investigate the detachment of mitochondria-bound HK-II, HeLa cells were treated with 12.5 μM of the peptides pFL-LP1-TAT, Pal-LP1-TAT, and Pal-LP1-RVR for a period of 4 hours (Figure 5b). Images were acquired using a laser scanning confocal microscope. The colocalization of the predominant green fluorescence (HK-II labeled with FITC) and red fluorescence (Mito Tracker) in the control cells indicated the distribution of HK-II on the mitochondria. However, a portion of the green fluorescence signal in the treated cells did not colocalize with the red fluorescence signals, suggesting the detachment of HK-II from the mitochondria. Therefore, it can be concluded that the designed VDAC1-based amphiphilic cationic peptides target the mitochondria, detach HK-II from these organelles, and subsequently trigger apoptosis in HeLa cells. We hypothesize that LP1, or the modified LP1 peptide released from the nanofiber assemblies, competes with HK-II for binding to VDAC1, potentially displacing HK-II from this binding site. Furthermore, it is plausible that the binding of the peptides to VDAC1 induces conformational changes that allosterically reduce the binding affinity of HK-II. Overall, this mechanism appears to involve the disruption of the protein-protein interaction interface. The peptides may directly interact with the binding interface between VDAC1 and HK-II, physically hindering their association.

The results obtained demonstrate the detachment of HK-II from the mitochondria, as observed using confocal microscopy following treatment with the peptides. This finding supports the notion of the disrupted VDAC1-HK-II complex formation, given that HK-II is typically bound to VDAC1 on the outer mitochondrial membrane.

To elucidate the mechanism of apoptosis following the targeting of cell mitochondria by peptides and the subsequent detachment of HK-II from the mitochondria, changes in mitochondrial membrane potential (MMP) were assessed using JC-1 dye via confocal fluorescence microscopy (Figure 6a). A decrease in mitochondrial membrane potential is recognized as one of the most critical markers of early apoptosis. JC-1, a cationic cyanine dye, enters healthy mitochondria in a potential-dependent manner, forming aggregates that emit red fluorescence. Conversely, when the mitochondrial membrane potential decreases, JC-1 exists in a monomeric form in the cytoplasm,

producing green fluorescence. Compared to the control group, HeLa cells treated with 12.5 μM peptides pFL-LP1-TAT, Pal-LP1-TAT, and Pal-LP1-RVR for 4 hours exhibited increased green fluorescence and decreased red fluorescence, indicating a reduction in mitochondrial membrane potential. This finding suggests that mitochondria-mediated apoptosis is initiated by the studied VDAC1-based peptides. Notably, the intensity of red fluorescence in Pal-LP1-TAT-treated cells was weaker than that in pFL-LP1-TAT-treated cells. Furthermore, the intensity of red fluorescence in Pal-LP1-RVR-treated cells was the weakest, which aligns with the observed apoptosis results. The release of cytochrome c was assessed using an immunofluorescence method (Figure 6b). HeLa cells were treated with 12.5 μM peptides pFL-LP1-TAT, Pal-LP1-TAT, and Pal-LP1-RVR for 4 hours. In the control group, there was a notable colocalization of green [Cyto-c (FITC)] and red fluorescence (Mito Tracker), indicating the distribution of cytochrome c within the mitochondria. In contrast, in peptide-treated cells, some green fluorescence signals did not colocalize with the red fluorescence signals, suggesting the release of cytochrome C from the mitochondria.

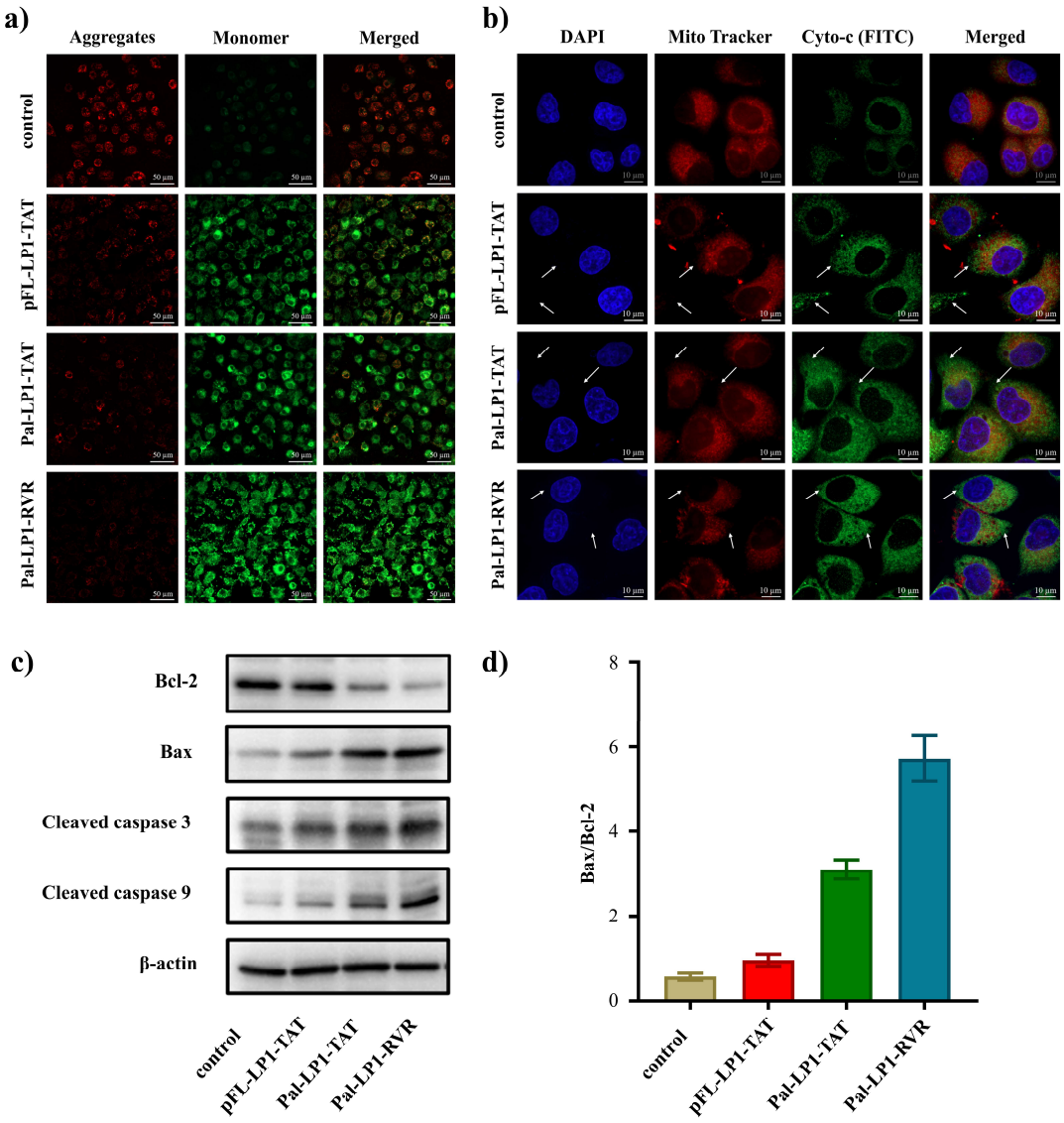

Figure 6. a) Changes in the mitochondrial membrane potential (MMP) of HeLa cells that were treated with peptides (12.5 μM) for 4 h. b) Detection of cytochrome c release of HeLa cells treated with peptides for 4 h. The blue channel shows the location of the cell nucleus. The green channel is associated with cytochrome C by immunostaining. The red channel shows the location of the stained mitochondria. The arrows indicate cytochrome C release. c) and d) Changes in the expression levels of apoptosis-associated proteins in HeLa cells treated with peptides for 24 h.

The expression of apoptosis-associated proteins, particularly in the context of mitochondria-mediated apoptosis, was assessed using Western Blot analysis (Figure 6c). HeLa cells were treated

with 12.5 μM of peptides pFL-LP1-TAT, Pal-LP1-TAT, and Pal-LP1-RVR for 24 hours, after which the proteins were extracted. Bcl-2 family proteins, comprising both pro-apoptotic and anti-apoptotic proteins, are recognized as critical markers in the progression of apoptosis. Figures 6c and 6d demonstrate an increase in Bax expression and a significant decrease in Bcl-2 expression in the peptide-treated HeLa cells, resulting in a notable increase in the Bax/Bcl-2 ratio. Additionally, the expression levels of cleaved caspase 9 and cleaved caspase 3 proteins were significantly elevated compared to the control group. These findings indicate that the process of mitochondria-mediated apoptosis is indeed activated, and the expression of apoptosis-associated proteins aligns with the observed apoptotic outcomes.

The decrease in mitochondrial membrane potential, the release of cytochrome c, the increased expression levels of Bax, cleaved caspase 9, and cleaved caspase 3, along with the decreased expression of Bcl-2 in HeLa cells treated with the designed amphiphilic cationic peptides, provide evidence that cell death is induced by mitochondria-mediated apoptosis.

Inhibitory effect of the peptides on tumors in mice

Tumor volume results post-treatment of a mouse model by peptides are shown in Figure S2. The animal experiment was conducted among the control group, the Pal-LP1-TAT peptide group, and the Pal-LP1-RVR peptide group, focusing on tumor growth and changes in body weight. The tumor images in Fig. S2a revealed that the tumor volume in the control group was significantly larger than that in the experimental groups treated with Pal-LP1-TAT and Pal-LP1-RVR peptides 10 days after administration. The tumor volumes in the Pal-LP1-TAT and Pal-LP1-RVR groups were relatively smaller, with the Pal-LP1-RVR group demonstrating a more pronounced tumor suppression effect. The tumor volume curves in Fig. S2b further confirmed this result, indicating stronger activity of the Pal-LP1-RVR peptide in inhibiting tumor growth. The data in Fig. S2c indicated that there was no significant downward trend in body weight across all three groups throughout the experiment. These results underscored the promising antitumor efficacy and safety of Pal-LP1-TAT and Pal-LP1-RVR peptides *in vivo*, providing the fundamental evidence for their potential development as anticancer therapeutic agents.

Figure 7 summarizes the suggested pathway of the biological activity of VDAC1-based amphiphilic cationic peptides inducing apoptosis in HeLa cells. These peptides target the

mitochondrial membranes of cancer cells and facilitate the detachment of HK-II from the OMM. This action triggers mitochondria-mediated apoptosis, leading to depolarization of the mitochondrial membrane potential and the release of cytochrome c. Subsequently, the expression of apoptosis-associated proteins is altered, with an increase in Bax, cleaved caspase 9, and cleaved caspase 3, alongside a decrease in Bcl-2 protein levels. All of these results indicate the occurrence of cell apoptosis. Therefore, the development of VDAC1-based amphiphilic cationic peptides with potent anticancer properties may offer new prospects for cancer therapy.

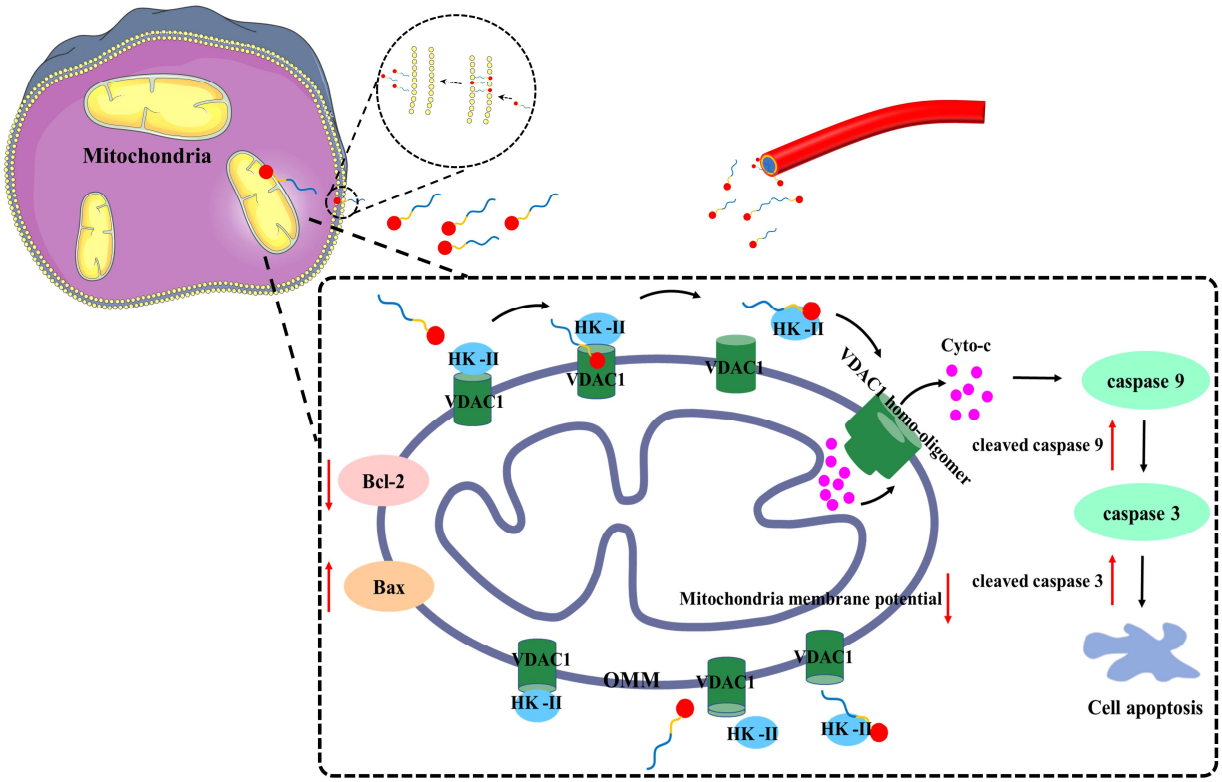

Figure 7. Proposed mechanism of action of mitochondrial VDAC1-derived amphiphilic peptides in cancer cells. The amphiphilic peptides penetrate the plasma cellular membrane thanks to their cell-penetrating properties and facilitate the dissociation of the VDAC1-HK-II complex overexpressed in the cancer cells. This triggers the activation of mitochondrial-mediated apoptosis. Self-assembly of monomeric peptides into nanofibers can occur in the aqueous environment above a critical concentration. Peptide nanofibers (formed at high concentrations) act as reservoirs and can release bioactive peptide monomers to translocate the lipid membranes in mitochondria-targeting experiments.

CONCLUSION

VDAC1 protein is overexpressed in various cancer cells, and its interaction with HK-II promotes cell proliferation while inhibiting apoptosis. In this study, we designed a series of VDAC1-based amphiphilic cationic peptides aimed as anticancer agents through the inhibition of protein-protein interactions in the apoptosis pathway. The peptides pFL-LP1-TAT, Pal-LP1-TAT, and Pal-LP1-RVR were derived from the VDAC1-based peptide LP1, incorporating positively charged peptides and hydrophobic building blocks. When introduced into PBS aqueous medium, the hydrophobic portions of these peptide molecules preferentially assemble into aggregates to minimize their exposure to water, while the hydrophilic regions remain exposed. This behavior results in significant amphiphilicity of the peptides and their self-assembly into nanofibers at concentrations above the CMC. The nanofibers can act as reservoirs of bioactive peptide monomers. The secondary structure of the designed peptides includes partial α-helical conformations, with Pal-LP1-RVR exhibiting a higher degree of helicity, suggesting a stronger interaction with lipid membranes. The studied peptides demonstrate lower IC_{50} values against HeLa cells compared to the control peptides LP1, indicating a correlation between the molecular characteristics of the designed peptides and their anticancer efficacy. Additionally, the peptides exhibited minimal cytotoxicity towards normal 3T3 cells, implying selective cytotoxicity. Furthermore, the designed peptides induced apoptosis in HeLa cells by binding to mitochondria and dissociating HK-II from these organelles, thereby triggering mitochondria-mediated apoptosis and altering the expression of apoptosis-related proteins. Notably, the decrease of the mitochondrial membrane potential resulted in the release of cytochrome C and the activation of caspase family proteins. In conclusion, the VDAC1-based amphiphilic cationic peptides exhibit remarkable anticancer activity and safety, signifying that the peptide sequences pFL-LP1-TAT, Pal-LP1-TAT, and Pal-LP1-RVR hold promise for the development of anticancer therapeutics targeting the mitochondrial VDAC1-HK-II complex. The reported findings suggest that the novel amphiphilic peptides targeting the VDAC1-HK-II complex may offer a new strategy for treating cervical cancer.

EXPERIMENTAL SECTION

Reagents and Materials. The designed peptides were custom synthesized by Nanjing Peptide Biotech Ltd (China) with purity > 95%. Phosphate Buffered Saline (PBS) was purchased from Shanghai Double-Helix Biotech Co., Ltd (China). Dimethyl sulfoxide (DMSO), 3-(4,5-Dimethylthiazol-2-yl)-2,5-diphenyltetrazolium bromide (MTT) kit, JC-1 kit, and Mito Tracker Deep Red FM were purchased from MKBio (China). Annexin V-FITC/PI apoptosis detection kit was purchased from Sangon Biotech (Shanghai) Co., Ltd. Dulbecco's modified Eagle's medium (DMEM), fetal bovine serum, and 0.25% trypsin−EDTA were purchased from Gibco (USA). Caspase 3 rabbit pAb, caspase 9 rabbit pAb, β-actin rabbit mAb, HRP goat-anti-rabbit IgG (H+L), and FITC goat-anti-rabbit IgG (H+L) were purchased from ABclonal (China). HK-II rabbit pAb, Bcl-2 rabbit pAB, Bax rabbit pAb and cytochrome c rabbit pAb were purchased from Proteintech Group, Inc Rosement, IL 60018 (USA). Antifade solution [4',6-diamidino-2-phenylindole (DAPI)] was purchased from Beyotime (China). Omni-PAGETM Hepes-Tris Gels and the Omni-ECLTM Femto Light Chemiluminescence Kit were purchased from EpiZyme (China). All compounds are > 95% pure by HPLC analysis (Fig S3).

Custom Peptide Synthesis. The designed peptides were synthesized using Standard Fmoc Solid Phase Techniques. Reverse-phase high-performance liquid chromatography (Hanbon, NP7005C, China) with a Kromasil C18 column was employed to isolate and purify the crude peptides. Mobile phases of HPLC consist of solvent A (0.1% TFA in acetonitrile) and solvent B (0.1% TFA in water), and a liner gradient was obtained from 20 to 100% solvent A. Purity and mass were determined by high performance liquid chromatography mass spectrometry (SHIMADZU, LCMS-2020, Japan), respectively. The purity of all peptides was more than 98%, and the peptide was stored at -20 ℃ until using.

Transmission Electron Microscopy (TEM). TEM experiments were performed at the National Center for Protein Science Shanghai (China) on a Tecnai G2 Spirit Twin TEM. The samples were prepared by the negative staining method. First, sample solution (5 μL) was placed onto a copper grid with carbon Formvar-coating. After adsorption for 1-2 min, the excess fluid was removed by the filter paper. The grid was then placed onto a drop of uranyl acetate solution (2% w/v) and stained for 1-2 min. The samples were imaged at an acceleration voltage of 120 kV.

CD Analysis. The circular dichroism (CD) spectra of all peptides (0.2 mM) were measured at 25℃ on a Jasco J-810 spectrometer (JascoCo., Japan) employing a quartz cell with a pathlength of 1 mm. The spectra were recorded in the UV range of 190-260 nm at a scan rate of 1 $nm \cdot s^{-1}$. The measurements were performed three times. The content of various secondary structures of the peptides in aqueous solutions was calculated using Bestsel (https://bestsel.elte.hu/results.php) and Dichroweb (http://dichroweb.cryst.bb k.ac.uk /html/process.shtml).

Cytotoxicity Assay. Cell viability was measured via the MTT assay. First, 100 μL of cells in the logarithmic growth phase were seeded in 96 wells plate at the cell concentration of 5×10^3cells per well. Cells were allowed to be adherent at 37 °C for 24 h. Then the medium was removed and the cells were washed by PBS. The serum-free DMEM medium with peptides at concentration of 0,

3.125, 6.25, 12.5, 25, 50 μM was added to the wells (100 μL per well). After incubation at 37 °C for 24 h, 10 μL of MTT reagent (5 mg/mL) was added to each well and cells were further incubated at 37 °C for 4 h. The solution was removed and DMSO (100 μL) was added to each well. OD values were measured at 492 and 630 nm. The viability was calculated using the following formula: viability (%) = (mean OD value of treatment group-blank) / (mean OD value of control group-blank) × 100%. The IC_{50} values were analyzed by GraphPad Prism 8.

Cell Apoptosis Assays. The Annexin V-FITC/PI apoptosis detection kit was used to detect the cell apoptosis rate on a BD LSRFortessa Flow Cytometer (BD Biosciences, USA). Cells were seeded in six-well plates at the concentration of 1×10^5 cells per mL and were incubated for 24 h at 37 °C. Afterward, the medium was removed and the cells were washed by PBS. The serum-free DMEM medium with the peptides (12.5 μM) was added to the wells for 4 h. After that, cells were detached and collected by centrifugation. The cell suspensions were incubated with binding buffer (300 μL) and Annexin V-FITC (10 μL) for 20 min as well as PI (5 μL) for 5 min in the dark. The fluorescence of Annexin V-FITC was excited at a wavelength of 488 nm and its emission was recorded at 530 nm, while Propidium Iodide (PI) was excited at 561 nm and its emission was recorded at 575 nm.

Intracellular Colocalization Study. Intracellular colocalization experiment was performed under a Zeiss SD confocal laser scanning microscope (Zeiss, Germany). Cells were seeded in glass bottom dishes (In Vitro Scientific, U.S.) at the concentration of 1×10^4 cells per mL for 12h and were treated with the studied peptides (12.5 μM) which were labeled by FITC for 4 h. Then, cells were incubated with 100 nM Mito Tracker Deep Red FM for 45 min at 37°C to stain the mitochondria. The fluorescence measurements were conducted at excitation wavelengths of 488 and 633 nm and emission was recorded at 530 nm and 697 nm for the FITC-conjugated peptides and Mito Tracker Deep Red FM, respectively. Using ZEN software to process the image.

Immunofluorescence Staining. Cells were seeded in a 20 mm glass bottom dish at the concentration of 5×10^4 cell per mL and incubated for 24 h. Then, the cells were subjected to peptides (12.5 μM) for 4 h at 37°C. After incubation, cells were washed with PBS, fixed with 4% paraformaldehyde for 25 min, permeabilized with 3% BSA with 0.1% Triton X-100 for 30 min, incubated with HK-II rabbit polyclonal antibody or Cyto-c rabbit polyclonal antibody at 1:50 for 2 h, washed with PBS-0.5% Triton X-100, then incubated with FITC goat-anti-rabbit IgG at 1:200 for 30 min, washed with PBS-0.5% Triton X-100. Finally, the cells were stained with Mito Tracker Deep Red FM (1 mM, 45 min) and antifade solution with DAPI. The cells were imaged by Zeiss SD laser scanning confocal microscope.

Mitochondrial Membrane Potential Assay. Depolarization of the mitochondrial membrane potential was measured using the fluorescent probe JC-1 kit. Cells were seeded into a 20 mm glass bottom dish at the density of 5×10^4 cell per mL for 24 h, and treated with peptides (12.5 μM) for 4 h. Thereafter, cells were washed with cold PBS and incubated with JC-1 staining solution at 37°C for 20 min in dark. Then, washing cells with cold JC-1 staining buffer. Fresh DMEM was added and imaging was performed on Zeiss SD laser scanning confocal microscope. JC-1 monomers was excited at 488 nm and the emission was recorded at 530 nm, JC-1 aggregates was excited at 561 nm and the emission was recorded at 590 nm.

Western Blot. Cellular proteins were extracted by the Column Tissue and Cell Protein Extraction Kit (Epizyme, China). The expression level of apoptosis proteins was analyzed by western blot. Briefly, cells were seed in the 10 cm dish for 24 h, treated with peptides (12.5 μM) for 24 h. Washing Cells using cold PBS, and adding the lysis buffer with protease inhibitor for 3 min. Then, lysates were collected in the cold purification tubes and centrifuged at 15000 rpm for 30 s. The concentration of protein was measured using Instant BCA Protein Assay Kit (Epizyme, China). After that, electrophoresis of the samples was carried out and samples were transferred to the polyvinylidene difluoride membrane. The membrane was closed, incubated with the samples rabbit antihuman antibodies overnight at 4 ℃, HRP goat-anti-rabbit IgG (H+L) for 30 min. Samples were visualized by Omni-ECL Femto light chemiluminescence kit (Epizyme Biotech, China) on the ChemiDoc MP imaging system (Bio-Rad, USA).

Peptides inhibit tumor growth in vivo. Hela cells were injected under the skin of 5-week-old nude mice (1×10^6 cells in 100 μL PBS). Mice with tumors were split into three groups: control (PBS injections), experimental (100μL 10 mg/kg peptide Pal-LP1-TAT and Pal-LP1-RVR). Treatments ran for 10 days. Tumor size was tracked every 2 days using calipers, with volume calculated as (length × width²)/2. Final tumor volumes and weights were compared to calculate growth inhibition. All animal work followed IACUC ethics standards.

ASSOCIATED CONTENT

Supporting Information

Additional figures with data about the properties of the amphiphilic peptides and inhibitory effect of the peptides on tumors in mice. Fig. S1 Critical micelle concentrations of the peptides a) pFL-LP1-TAT, b) Pal-LP1-TAT, and c) Pal-LP1-RVR, determined using a pyrene fluorescent probe in PBS (pH 7.4). Table S1 α-helical content (%) of peptides at different concentrations in the aqueous phase calculated by Bestsel. Table. S2 α-helical content (%) of peptides at different concentrations in the aqueous phase calculated by Dichroweb. Table. S3 Ratio of the molar ellipticity $\theta_{222}/\theta_{208}$ of peptides at different concentrations in the aqueous phase. Table. S4 Summary of the half maximal inhibitory concentration (IC_{50}) values (μM) for cell death induction by the novel amphiphilic self-assembled antitumor peptides in various cancer cell lines. Fig. S2 Tumor volume results post-treatment by a control peptide Pal-LP1-TAT and a cationic amphiphilic peptide Pal-LP1-RVR in mice, a) representative images of tumors obtained from mouse after 10 days of administration, b) tumor volume curve, c) mouse weight curve. Fig. S3 HPLC Chromatogram of a) pFL-LP1-TAT (500 μM), b) Pal-LP1-TAT (500 μM) and c) Pal-LP1-RVR (500 μM). Fig S4. CD spectra of multi-block peptides at 0.1mM in the aqueous phase: a) pFL-LP1-TAT, b) Pal-LP1-TAT and c) Pal-LP1-RVR.

AUTHOR INFORMATION

Corresponding author. *E-mail address: nli@sibcb.ac.cn

Corresponding author. *E-mail address: aihuazou@shnu.edu.cn

Author Contributions

The manuscript was written through contributions of all authors. All authors have given approval to the final version of the manuscript.

Notes

The authors declare no competing financial interest.

Funding Sources

This work was supported by the National Natural Science Foundation of China [nos. 22334006]. B.A. was funded by the project "Structural dynamics of biomolecular systems (ELIBIO)" (No. CZ.02.1.01/0.0/0.0/15_003/0000447) from the European Regional Development Fund, by the Czech Science Foundation (GACR project No. 24-10671S), and the Johannes Amos Comenius Operational Program OPJAK (project No. SENDISO CZ.02.01.01/00/22_008/0004596).

ACKNOWLEDGMENT

We thank Dr. Shuyang Tu from the Shanghai Advanced Research Institute for helping with the experiment of cell membrane local heterogeneity characterization. We thank the staffs of National Facility for Protein Science in Shanghai (NFPS) for assistance during data collection of TEM, confocal microscopy, and flow cytometer. A.A. acknowledges a membership in the CNRS GDR2088 BIOMIM research network.

REFERENCES

(1) Lim, W. Q.; Yang, G.; Phua, S. Z. F.; Chen, H.; Zhao, Y. Self-Assembled Oxaliplatin(IV) Prodrug–Porphyrin Conjugate for Combinational Photodynamic Therapy and Chemotherapy. *ACS Appl. Mater. Interfaces* **2019**, *11* (18), 16391–16401. https://doi.org/10.1021/acsami.9b04557.

(2) Kim, J.; Jo, C.; Lim, W.-G.; Jung, S.; Lee, Y. M.; Lim, J.; Lee, H.; Lee, J.; Kim, W. J. Programmed Nanoparticle-Loaded Nanoparticles for Deep-Penetrating 3D Cancer Therapy. *Advanced Materials* **2018**, *30* (29), 1707557. https://doi.org/10.1002/adma.201707557.

(3) Qu, Y.; Jin, W.; Wan, Y.; Pei, Z.; Pei, Y. J-Aggregation of Photosensitizers Leads to an Ultrahigh Drug-Loading System for Targeted Delivery. *Chinese Chemical Letters* **2024**, *35* (1), 108493. https://doi.org/10.1016/j.cclet.2023.108493.

(4) Deepagan, V. G.; Ko, H.; Kwon, S.; Rao, N. V.; Kim, S. K.; Um, W.; Lee, S.; Min, J.; Lee, J.; Choi, K. Y.; Shin, S.; Suh, M.; Park, J. H. Intracellularly Activatable Nanovasodilators To Enhance Passive Cancer Targeting Regime. *Nano Lett.* **2018**, *18* (4), 2637–2644. https://doi.org/10.1021/acs.nanolett.8b00495.

(5) Li, L.-L.; Qiao, Z.-Y.; Wang, L.; Wang, H. Self-Assembly: Programmable Construction of Peptide-Based Materials in Living Subjects: From Modular Design and Morphological Control to Theranostics (Adv. Mater. 45/2019). *Advanced Materials* **2019**, *31* (45), 1970321. https://doi.org/10.1002/adma.201970321.

(6) Fu, D.; Liu, D.; Zhang, L.; Sun, L. Self-Assembled Fluorescent Tripeptide Nanoparticles for Bioimaging and Drug Delivery Applications. *Chinese Chemical Letters* **2020**, *31* (12), 3195–3199. https://doi.org/10.1016/j.cclet.2020.07.011.

(7) Chen, Z.; Zhang, K.; Fan, J.; Fan, Y.; Yang, C.; Tian, W.; Li, Y.; Li, W.; Zhang, J.; Wang, H.; Wang, L. *In Situ* Construction of Ligand Nano-Network to Integrin $\alpha v\beta 3$ for Angiogenesis Inhibition. *Chinese Chemical Letters* **2020**, *31* (12), 3107–3112. https://doi.org/10.1016/j.cclet.2020.04.006.

(8) Fan, J.; Fan, Y.; Wei, Z.; Li, Y.; Li, X.; Wang, L.; Wang, H. Transformable Peptide Nanoparticles Inhibit the Migration of N-Cadherin Overexpressed Cancer Cells. *Chinese Chemical Letters* **2020**, *31* (7), 1787–1791. https://doi.org/10.1016/j.cclet.2020.03.065.

(9) Yang, H.; Xiong, Y.; Li, M.; Yang, Z.; Meng, P.; Qing, G. Self-Assembly of Phosphorylated Peptide Driven by Dy3+. *Chinese Chemical Letters* **2023**, *34* (8), 108106. https://doi.org/10.1016/j.cclet.2022.108106.

(10) Chen, Z.; Xing, L.; Fan, Q.; Cheetham, A. G.; Lin, R.; Holt, B.; Chen, L.; Xiao, Y.; Cui, H. Drug-Bearing Supramolecular Filament Hydrogels as Anti-Inflammatory Agents. *Theranostics* **2017**, *7* (7), 2003–2014. https://doi.org/10.7150/thno.19404.

(11) Belostozky, A.; Richman, M.; Lisniansky, E.; Tovchygrechko, A.; Chill, J. H.; Rahimipour, S. Inhibition of Tau-Derived Hexapeptide Aggregation and Toxicity by a Self-Assembled Cyclic D,L-α-Peptide Conformational Inhibitor. *Chem. Commun.* **2018**, *54* (47), 5980–5983. https://doi.org/10.1039/C8CC01233D.

(12) Liu, N.; Zhu, L.; Li, Z.; Liu, W.; Sun, M.; Zhou, Z. In Situ Self-Assembled Peptide Nanofibers for Cancer Theranostics. *Biomater. Sci.* **2021**, *9* (16), 5427–5436. https://doi.org/10.1039/D1BM00782C.

(13) Shi, J.; Fichman, G.; Schneider, J. P. Enzymatic Control of the Conformational Landscape of Self-Assembling Peptides. *Angewandte Chemie International Edition* **2018**, *57* (35), 11188–11192. https://doi.org/10.1002/anie.201803983.

(14) Qiao, Z.-Y.; Zhao, W.-J.; Gao, Y.-J.; Cong, Y.; Zhao, L.; Hu, Z.; Wang, H. Reconfigurable Peptide Nanotherapeutics at Tumor Microenvironmental pH. *ACS Appl. Mater. Interfaces* **2017**, *9* (36), 30426–30436. https://doi.org/10.1021/acsami.7b09033.

(15) Pathak, R. K.; Marrache, S.; Harn, D. A.; Dhar, S. Mito-DCA: A Mitochondria Targeted Molecular Scaffold for Efficacious Delivery of Metabolic Modulator Dichloroacetate. *ACS Chem. Biol.* **2014**, *9* (5), 1178–1187. https://doi.org/10.1021/cb400944y.

(16) Sun, Y.; Zhang, H.; Lu, G.; Wang, H.; Lu, Y.; Fan, L. Mitochondria-Targeted Cancer Therapy Based on Functional Peptides. *Chinese Chemical Letters* **2023**, *34* (5), 107817. https://doi.org/10.1016/j.cclet.2022.107817.

(17) He, S.-F.; Pan, N.-L.; Chen, B.-B.; Liao, J.-X.; Huang, M.; Qiu, H.-J.; Jiang, D.-C.; Wang, J.-J.; Chen, J.-X.; Sun, J. Mitochondria-Targeted Re(I) Complexes Bearing Guanidinium as Ligands and Their Anticancer Activity. *J Biol Inorg Chem* **2020**, *25* (8), 1107–1116. https://doi.org/10.1007/s00775-020-01827-7.

(18) He, Y.; Fang, X.; Shi, J.; Li, X.; Xie, M.; Liu, X. Apigenin Attenuates Pulmonary Hypertension by Inducing Mitochondria-Dependent Apoptosis of PASMCs via Inhibiting the Hypoxia Inducible Factor 1α–KV1.5 Channel Pathway. *Chemico-Biological Interactions* **2020**, *317*, 108942. https://doi.org/10.1016/j.cbi.2020.108942.

(19) Aly, H. A. A.; Eid, B. G. Cisplatin Induced Testicular Damage through Mitochondria Mediated Apoptosis, Inflammation and Oxidative Stress in Rats: Impact of Resveratrol. *Endocrine Journal* **2020**, *advpub*, EJ20-0149. https://doi.org/10.1507/endocrj.EJ20-0149.

(20) No, M.-H.; Choi, Y.; Cho, J.; Heo, J.-W.; Cho, E.-J.; Park, D.-H.; Kang, J.-H.; Kim, C.-J.; Seo, D. Y.; Han, J.; Kwak, H.-B. Aging Promotes Mitochondria-Mediated Apoptosis in Rat Hearts. *Life* **2020**, *10* (9), 178. https://doi.org/10.3390/life10090178.

(21) Fulda, S. Shifting the Balance of Mitochondrial Apoptosis: Therapeutic Perspectives. *Frontiers in Oncology* **2012**, *2, 121.* https://doi.org/10.3389/fonc.2012.00121 .

(22) Kudryavtseva, A. V.; Fedorova, M. S.; Zhavoronkov, A.; Moskalev, A. A.; Zasedatelev, A. S.; Dmitriev, A. A.; Sadritdinova, A. F.; Karpova, I. Y.; Nyushko, K. M.; Kalinin, D. V.; Volchenko, N. N.; Melnikova, N. V.; Klimina, K. M.; Sidorov, D. V.; Popov, A. Y.; Nasedkina, T. V.; Kaprin, A. D.; Alekseev, B. Y.; Krasnov, G. S.; Snezhkina, A. V. Effect of Lentivirus-Mediated shRNA Inactivation of HK1, HK2, and HK3 Genes in Colorectal Cancer and Melanoma Cells. *BMC Genetics* **2016**, *17* (3), 156. https://doi.org/10.1186/s12863-016-0459-1.

(23) Patra, K. C.; Wang, Q.; Bhaskar, P. T.; Miller, L.; Wang, Z.; Wheaton, W.; Chandel, N.; Laakso, M.; Muller, W. J.; Allen, E. L.; Jha, A. K.; Smolen, G. A.; Clasquin, M. F.; Robey, R. B.; Hay, N. Hexokinase 2 Is Required for Tumor Initiation and Maintenance and Its Systemic Deletion Is Therapeutic in Mouse Models of Cancer. *Cancer Cell* **2013**, *24* (3), 399. https://doi.org/10.1016/j.ccr.2013.08.029.

(24) Shoshan-Barmatz, V.; Ben-Hail, D.; Admoni, L.; Krelin, Y.; Tripathi, S. S. The Mitochondrial Voltage-Dependent Anion Channel 1 in Tumor Cells. *Biochimica et Biophysica Acta (BBA) - Biomembranes* **2015**, *1848* (10, Part B), 2547–2575. https://doi.org/10.1016/j.bbamem.2014.10.040.

(25) Barnard, A.; Long, K.; Martin, H. L.; Miles, J. A.; Edwards, T. A.; Tomlinson, D. C.; Macdonald, A.; Wilson, A. J. Selective and Potent Proteomimetic Inhibitors of Intracellular Protein–Protein Interactions. *Angewandte Chemie International Edition* **2015**, *54* (10), 2960–2965. https://doi.org/10.1002/anie.201410810.

(26) Fosgerau, K.; Hoffmann, T. Peptide Therapeutics: Current Status and Future Directions. *Drug Discovery Today* **2015**, *20* (1), 122–128. https://doi.org/10.1016/j.drudis.2014.10.003.

(27) Liu, D.; Angelova, A.; Liu, J.; Garamus, V. M.; Angelov, B.; Zhang, X.; Li, Y.; Feger, G.; Li, N.; Zou, A. Self-Assembly of Mitochondria-Specific Peptide Amphiphiles Amplifying Lung Cancer Cell Death through Targeting the VDAC1–Hexokinase-II Complex. *J. Mater. Chem. B* **2019**, *7* (30), 4706–4716. https://doi.org/10.1039/C9TB00629J.

(28) Zhang, X.; Angelova, A.; Sun, W.; Zhang, F.; Li, N.; Zou, A. A Lipidated Peptide with Mitochondrial Membrane Localization in Human A549 Lung Cells: From Enhanced Cell-Penetrating Properties to Biological Activity Mechanism. *ACS Appl. Bio Mater.* **2021**, *4* (12), 8277–8290. https://doi.org/10.1021/acsabm.1c00815.

(29) Arzoine, L.; Zilberberg, N.; Ben-Romano, R.; Shoshan-Barmatz, V. Voltage-Dependent Anion Channel 1-Based Peptides Interact with Hexokinase to Prevent Its Anti-Apoptotic Activity *. *Journal of Biological Chemistry* **2009**, *284* (6), 3946–3955. https://doi.org/10.1074/jbc.M803614200.

(30) Prezma, T.; Shteinfer, A.; Admoni, L.; Raviv, Z.; Sela, I.; Levi, I.; Shoshan-Barmatz, V. VDAC1-Based Peptides: Novel pro-Apoptotic Agents and Potential Therapeutics for B-Cell Chronic Lymphocytic Leukemia. *Cell Death Dis* **2013**, *4* (9), e809–e809. https://doi.org/10.1038/cddis.2013.316.

(31) Pittala, S.; Krelin, Y.; Shoshan-Barmatz, V. Targeting Liver Cancer and Associated Pathologies in Mice with a Mitochondrial VDAC1-Based Peptide. *Neoplasia* **2018**, *20* (6), 594–609. https://doi.org/10.1016/j.neo.2018.02.012.

(32) Shteinfer-Kuzmine, A.; Amsalem, Z.; Arif, T.; Zooravlov, A.; Shoshan-Barmatz, V. Selective Induction of Cancer Cell Death by VDAC1-Based Peptides and Their Potential Use in Cancer Therapy. *Molecular Oncology* **2018**, *12* (7), 1077–1103. https://doi.org/10.1002/1878-0261.12313.

(33) Zhang, F.; Angelova, A.; Garamus, V. M.; Angelov, B.; Tu, S.; Kong, L.; Zhang, X.; Li, N.; Zou, A. Mitochondrial Voltage-Dependent Anion Channel 1–Hexokinase-II Complex-Targeted Strategy for Melanoma Inhibition Using Designed Multiblock Peptide Amphiphiles. *ACS Appl. Mater. Interfaces* **2021**, *13* (30), 35281–35293. https://doi.org/10.1021/acsami.1c04385.

(34) Xiang, S.; Hammer, B.; Kremer, K.; Müllen, K.; Weil, T. Engineering Surface Amphiphilicity of Polymer Nanostructures. *Progress in Polymer Science* **2022**, *124*, 101489. https://doi.org/10.1016/j.progpolymsci.2021.101489.

(35) Zhou, N. E.; Kay, C. M.; Hodges, R. S. Synthetic Model Proteins. Positional Effects of Interchain Hydrophobic Interactions on Stability of Two-Stranded Alpha-Helical Coiled-Coils. *Journal of Biological Chemistry* **1992**, *267* (4), 2664–2670. https://doi.org/10.1016/S0021-9258(18)45932-7.

(36) Li, Y.; Wang, Y.; Ou, S.-H.; Lock, L. L.; Xu, X.; Ghose, S.; Li, Z. J.; Cui, H. Conformation Preservation of α-Helical Peptides within Supramolecular Filamentous Assemblies. *Biomacromolecules* **2017**, *18* (11), 3611–3620. https://doi.org/10.1021/acs.biomac.7b00992.

(37) Wu, M.; Chen, Q.; Wang, Y.; Li, Y.; Zhao, X.; Chang, Q. Structural Modification and Antitumor Activity of Antimicrobial Peptide HYL. *Chinese Chemical Letters* **2020**, *31* (5), 1288–1292. https://doi.org/10.1016/j.cclet.2019.10.013.

Table of Contents Graphic

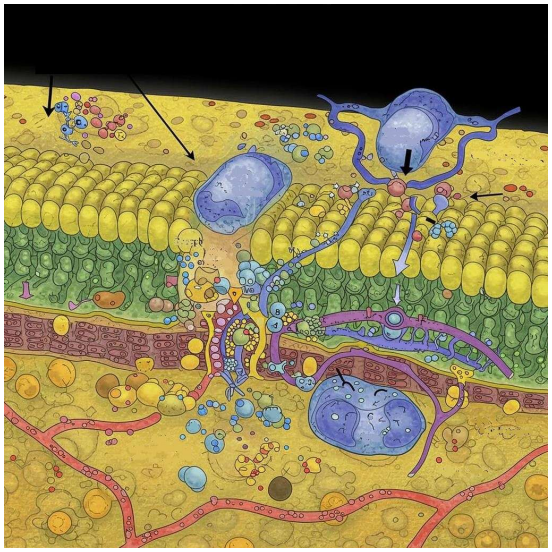

A designed amphiphilic cationic peptide traversing the cellular membrane of a cancer cell, overcoming one of the critical barriers in drug delivery, and aiming at specific intracellular targeting of the VDAC1-Hexokinase-II complex as a potential new strategy for the treatment of cervical cancer